ARTICLE

Spatial patterns of tree and shrub biomass in a deciduous forest using leaf-off and leaf-on lidar

Kristen M. Brubaker, Quincey K. Johnson, and Margot W. Kaye

Abstract: Understanding patterns of aboveground carbon storage across forest types is increasingly important as managers adapt to threats of global change. We combined field measures of aboveground biomass with lidar to model fine-scale biomass in deciduous forests located in two watersheds; one watershed was underlain by sandstone and the other by shale. We measured tree and shrub biomass across three topographic positions for both watersheds and analyzed biomass using mixed models. The watershed underlain by shale had 60% more aboveground biomass than the sandstone watershed. Although spatial patterns of biomass were different across watersheds, both had higher (between about 40% and 55%) biomass values at the toe-slope position than at the ridge-top position. To model fine-scale spatial patterns of biomass, we tested the effectiveness of leaf-on and leaf-off lidar combined with topographic metrics to develop a spatially explicit random forest model of tree and shrub biomass across both watersheds. Leaf-on variables were more important for modeling shrub biomass, while leaf-off variables were more effective at modeling tree biomass. Our model of tree and shrub biomass reflects the distribution of biomass across both watersheds at a fine scale and highlights the potential of abiotic factors such as topography and bedrock to affect carbon storage.

Key words: biomass, lidar, understory, carbon, shrub.

Résumé: Il est de plus en plus important de comprendre les profils de séquestration aérienne du carbone qui caractérisent les différents types de forêt alors que les gestionnaires s'adaptent aux menaces associées au changement global. Nous avons combiné des mesures de biomasse aérienne prises sur le terrain avec le lidar pour modéliser la biomasse à petite échelle dans des forêts décidues situées dans deux bassins versants : un des bassins reposait sur du grès et l'autre sur du schiste. Nous avons mesuré la biomasse des arbres et des arbustes dans trois positions topographiques dans les deux bassins et analysé la biomasse à l'aide de modèles mixtes. Le bassin qui reposait sur le schiste avait 60 % plus de biomasse aérienne que le bassin reposant sur le grès. Bien que la répartition spatiale de leur biomasse diffère, les deux bassins avaient des valeurs de biomasse plus élevées (environ 40 à 55 %) au pied qu'au sommet de la pente. Pour modéliser la répartition spatiale à petite échelle, nous avons testé l'efficacité du lidar en présence et en l'absence du feuillage jumelé à des données topographiques pour élaborer un modèle forestier aléatoire, spatialement explicite, de la biomasse arborescente et arbustive dans les deux bassins. Les variables mesurées en présence du feuillage étaient plus importantes pour modéliser la biomasse des arbustes tandis que les variables mesurées en l'absence du feuillage étaient plus efficaces pour modéliser la biomasse des arbres. Notre modèle de biomasse arbustive et arborescente reflète la répartition de la biomasse à petite échelle dans les deux bassins et met en évidence l'influence potentielle des facteurs abiotiques, tels que la topographie et le substrat rocheux, sur la séquestration du carbone. [Traduit par la Rédaction]

Mots-clés: biomasse, lidar, sous-bois, carbone, arbuste.

1. Introduction

Understanding patterns of carbon storage across forest types is increasingly important as managers adapt to the diverse threats of global change. Forests are vital components of the global carbon cycle and actively store and release carbon depending on many biotic and abiotic factors. Carbon stored in aboveground live and standing dead tree biomass can account for as much as 60% of the total terrestrial carbon sequestration in the Northern Hemisphere; however, this is highly variable across forests (Woodbury et al. 2007; Curtis 2008). Understanding the interaction and variation of biomass pools across space could allow forest managers to optimize carbon storage. Many factors are known to influence patterns and distribution of biomass pools, including vegetation community (Ruiz-Benito et al. 2014), forest structure (Duncanson et al. 2015), topography (Xu et al. 2015; Zald et al.

2016), climate (Iverson et al. 2008), and soil and parent material (de Castilho et al. 2006). On a local scale, total biomass, as well as the way that biomass is partitioned in an ecosystem, can differ significantly according to terrain (Smith et al. 2017; Bolstad et al. 2018) and soil characteristics (Tateno et al. 2004). Biomass at land-scape and broader scales (regional to national) has been modeled from forest inventory plots (Birdsey 1992; Brown et al. 1999), as well as fine-scale budgets on the order of one watershed (Smith et al. 2017), but spatial patterns of biomass pools across abiotic gradients are not well understood.

Topographic position and bedrock affect vegetation community composition and productivity through several different mechanisms. For example, trees tend to grow taller and contain more biomass in toe-slope positions, but it is not clear if this is due to water availability, nutrient availability, or an interaction of the two (McNab 1989; Bolstad et al. 1998; Tateno et al. 2004). Topo-

Received 2 February 2018. Accepted 12 June 2018.

K.M. Brubaker and Q.K. Johnson. Environmental Studies, Hobart and William Smith Colleges, 300 Pulteney St., Geneva, NY 14456, USA.

M.W. Kaye. Department of Ecosystem Science and Management, The Pennsylvania State University, 303 Forest Resources Building, University Park, PA 16802, USA.

Corresponding author: Kristen M. Brubaker (email: brubaker@hws.edu).

Copyright remains with the author(s) or their institution(s). Permission for reuse (free in most cases) can be obtained from RightsLink.

graphic factors that influence vegetation include hillslope position, slope, curvature (concavity or convexity of the site), hydrology, and aspect, among others (Swetnam et al. 2015). Bedrock also impacts vegetation communities through soil texture, nutrient holding capacity, and drainage rates (Hahm et al. 2014; Brantley et al. 2017). In the area of this study (northeastern United States), sandstone-derived soils tend to be excessively drained of both water and nutrients, which can limit plant growth, while shale-derived soils tend to be more productive (Ciolkosz et al. 1989). Spatial heterogeneity in forest biomass driven by topography and bedrock may require fine-scale (100 m² to 1 ha), spatially explicit models that take into account site-specific variables such as terrain.

Lidar has been used extensively to model landscape-scale tree biomass, ecosystem carbon values, and carbon fluxes (Hudak et al. 2012; Asner et al. 2012; Zolkos et al. 2013). Researchers have used a range of methods to model biomass, from individual-tree calculation and measurement (Zhao et al. 2009) to plot-level (Popescu and Wynne 2004; Hudak et al. 2008) and landscape-level (Wulder et al. 2012) assessments. Different statistical modeling techniques have been used, including parametric models (Lefsky et al. 1999), machine learning approaches including random forests (Gleason and Im 2012; Hudak et al. 2012), object-based classification (van Aardt et al. 2006), and single-tree detection algorithms (Popescu 2007; Brandtberg et al. 2003). Methods for lidar-based estimates of forest biomass are quickly advancing but inherently miss biomass pools beneath the canopy.

Shrub biomass may play an important role in terrestrial carbon budgets (Greaves et al. 2015; Li et al. 2015; Kristensen et al. 2015). Modelling shrub biomass in forested ecosystem, however, is difficult due to the presence of overstory tree canopies, which obscure the signal from the understory for both passive (Defibaugh y Chávez and Tullis 2013) and active (Hill and Broughton 2009) remote sensing techniques. Lidar has been used to model shrubs for habitat suitability (Vierling et al. 2008; Martinuzzi et al. 2009; Barber et al. 2016) and to model shrub presence or absence with up to 83% accuracy (Martinuzzi et al. 2009). Shrub presence or absence has also been modeled using lidar to determine invasive shrub presence in urban areas (Asner et al. 2008; Singh et al. 2015; Chance et al. 2016); however, few studies have modeled abundance or biomass of shrubs across the landscape (Gopalakrishnan et al. 2018). Also, many of the studies using lidar to model understories have been focused on more open coniferous or eucalypt forests (Wing et al. 2012; Barber et al. 2016; Hudak et al. 2016; Fedrigo et al. 2018) versus closed deciduous forests.

The purpose of this study is to further our understanding of how aboveground biomass pools differ across mixed deciduous forests and how to model these pools with lidar. Our objectives were to (i) calculate relative biomass pools for trees and shrubs in mixed deciduous forests, (ii) determine how leaf-on or leaf-off lidar data can be used to model tree and shrub biomass independently, and (iii) explore how abiotic factors such as bedrock and terrain can influence spatial patterns of tree and shrub biomass. For our lidar-based analysis, we chose a machine learning modeling approach with random forest because of its relatively robust ability to work with correlated variables and variables with nonnormal distributions (Breiman 2001; Cutler et al. 2007; Olden et al. 2008). Using fine-scale maps (10 m resolution) of tree and shrub biomass, we identified trends in biomass across varying landforms in watersheds with different bedrock types. The diversity of topographic and bedrock positions provides a range of abiotic and biotic conditions needed to capture spatial variability in aboveground biomass. We completed our study at the Susquehanna Shale Hills Critical Zone Observatory (CZO), which is an interdisciplinary observatory designed to study the creation and function of the critical zone, the region where bedrock intersects with the biosphere.

2. Materials and methods

2.1. Study area

This study took place in a mixed deciduous forest in the Susquehanna Shale Hills CZO in central Pennsylvania, USA, part of the National Critical Zone Observatory Network (Fig. 1). The National Critical Zone Observatory network includes nine environmental observatories designed to improve our understanding of how various aspects of the surface of the Earth interact. We collected data for two subwatersheds within the broader Shaver's Creek watershed described in detail by Brantley et al. (2016). Both watersheds were cleared of timber during the late 1800s to early 1900s, but there is no known recent timber harvesting in our study areas. Forests in both watersheds are about 100 years old, with those at Shale Hills potentially being slightly older (Brantley et al. 2016; Smith et al. 2017).

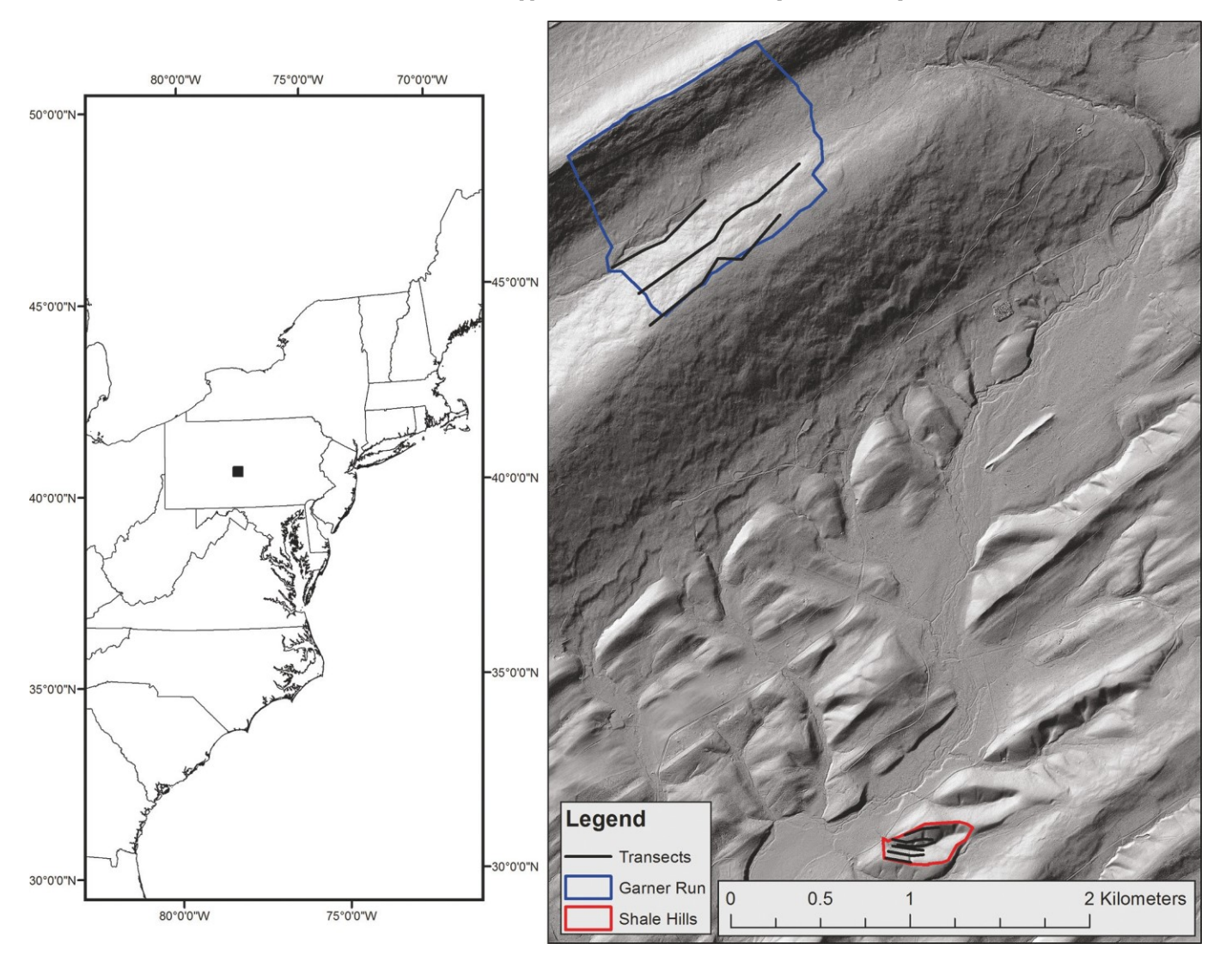
The first watershed, Shale Hills, is approximately 9 ha and contains a deciduous forest dominated by *Quercus rubra* L., *Quercus prinus* L. syn *Quercus montana* Willd., *Quercus alba* L., *Carya* spp., and *Acer saccharum* Marsh. The vegetation community type is oakmixed hardwood, which is a diverse forest that tends to be found on relatively mesic, rich soils in the region. It is characterized by a sparse understory. This watershed is underlain by shale bedrock of the Clinton group, and the soil types are Berks–Weikert associations. Elevation in the watershed ranges from 260 m to 300 m above sea level, and the watershed has both northern and southern aspects. Slopes in the midslope section of both northern and southern aspects of the watershed average about 32%, with a range between 18% and 45%.

The second watershed, Garner Run, is approximately 125 ha. It also contains relatively undisturbed second-growth forest on northern and southern aspects, with some tree harvesting having occurred on the southern aspect in an area excluded from our study. The watershed is underlain by sandstone of the Tuscarora formation. The forest type in this watershed is primarily a dry oak-heath type characterized by a less diverse overstory of Quercus montana, Acer rubrum L., Betula lenta L., and Nyssa sylvatica Marsh. The understory tends to have an abundance of both deciduous and evergreen shrubs, including Vaccinium spp. and Gaylussacia spp., and other members of the Ericaceous family such as Kalmia latifolia L. and Rhododendron maximum L. Elevation in the watershed ranges from 470 m to approximately 650 m above sea level. Slopes on the southern aspect at mid-slope average 35%, with a range between 10% and 60%, while slopes on the northern aspect at mid-slope average about 25%, with a range between 6% and 48%.

2.2. Methods overview

We used several methods to further our understanding of biomass pools and patterns of biomass across our watersheds, particularly with respect to topographic position and bedrock. Each method is described below in more detail. We used 10 m wide belt transects located parallel to slope contour at each topographic position in both watersheds to sample tree biomass. We sampled shrub biomass in smaller shrub plots along the belt transects. Using mean biomass values from each topographic position, as well as the relative area of the topographic positions in each watershed, average tree biomass and shrub biomass were estimated for each watershed. We then used linear mixed models to test the significance of watershed and topographic position on tree and shrub biomass. We finally used leaf-on and leaf-off lidar to build a spatial model of shrub and tree biomass across both watersheds. We used random forest regression to determine which leaf-on and leaf-off lidar variables were important for modeling tree and shrub biomass. Once we determined which model explained the maximum amount of variance for tree biomass and shrub biomass, we applied these models to our study area, allowing us to model biomass pools across topographic positions and watersheds.

Fig. 1. The location of the Susquehanna Shale Hills Critical Zone Observatory in Central Pennsylvania, USA, with the location and relative size of the Garner Run and Shale Hills watersheds and the approximate transect locations. [Colour online.]



2.3. Data sources

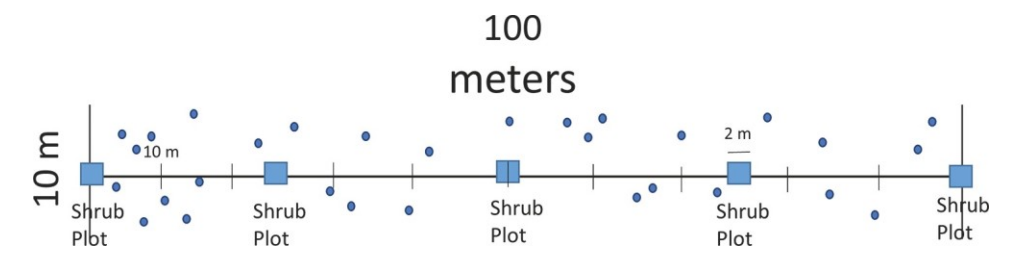
Lidar and field data were collected and used for this analysis. Field data were collected primarily during the summers of 2014 (trees, both watersheds) and 2015 (shrubs, both watersheds), and lidar data were collected in 2010. The earlier date of the lidar survey compared with the field measurements should not bias our results because the structure of these mature forests (>100 years old) is slow to change through time and light conditions for the understory are consistently low. Shrub biomass estimates only included understory species and not young regenerating trees. The shrub biomass was primarily from *Kalmia latifolia*, which is extremely slow growing in the region (Brose 2016). Tree biomass increased by ~3% per year across the Shale Hills Watershed during this time (Smith et al. 2017).

A stratified sampling plan was used to measure forest composition and structure at the two watersheds. We were particularly interested in understanding the role of abiotic factors and topographic position on patterns of biomass, so permanent transects were established as part of the CZO and marked to allow monitoring of vegetation at different topographic positions. Earlier lidarbased studies (Brubaker et al. 2014) have shown that tree height varies with respect to topographic position at our study locations, so we stratified our sampling scheme to ensure similar numbers

of plots across the range of biomass values in the watershed (Hawbaker et al. 2009). Linear transects were placed in the field in 50 m or 100 m segments, depending on the watershed. The starting point was established based on observed patterns of curvature in the field, and the transect was marked off following a compass reading that approximately paralleled the slope. At the end of each segment, the next segment was placed to again parallel the slope, so that each segment could have a different azimuth to follow the approximate terrain. Linear transects were sampled at toe-slope, mid-slope, and ridge-top positions to capture the diversity of topography in the watersheds and the variable terrain at each of the topographic positions (Fig. 1). We designed our sampling scheme to ensure that we were capturing adequate data across the range of biomass values in each watershed and also so that we could repeat our measures of the same trees to capture carbon fluxes in future studies.

In the Shale Hills watershed, six transects were measured: one transect for each topographic position (toe-slope, mid-slope, and ridge-top) on both the northern and southern aspects of the watershed (Fig. 1). Transects were 10 m wide and sampled in 50 m segments that followed the topographic position. The length of transects sampled ranged from 200 m to 250 m, and a total of 1.35 ha were sampled (15% of the watershed). The start points

Fig. 2. Schematic showing layout of tree (circles) and shrub (within squares) measurements measured at each 100 m segment of sampling transect for Garner Run. [Colour online.]



of transects were placed at the western and downstream end of the watershed where there is more space to avoid convergence of transects as we sampled in an eastward direction up the narrowing watershed. Estimated tree biomass in the watershed does not show a clear east-west trend (Smith et al. 2017) so sampling at multiple topographic positions in the western portion of the watershed captures the variability in biomass across the area.

Because Garner Run is a much larger watershed (125 ha), a slightly different sampling strategy was used (Brantley et al. 2016). The southern aspect at Garner Run tends to be steeper, with a greater range of elevation (Brantley et al. 2016) and shorter trees (Brubaker et al. 2014). Additionally, there had been recent timber harvesting on the lower slope position on the southern aspect of the watershed. Therefore, we set up four transects: toe-slope, midslope, and ridge-top transects on the northern aspect of the watershed and a mid-slope transect on the southern aspect of the watershed. These transects were 10 m wide and sampled in 100 m segment lengths, and the total length of transects ranged from about 800 m to over 1 km. A total of 4.1 ha was sampled (3.25% of the watershed area). In both watersheds, each transect segment end was georeferenced using a Trimble GeoXT with differential correction during leaf-off periods. Distances within transects were measured with a tape measuring from a permanent marker at each transect segment end.

All trees greater than 10 cm diameter at breast height (dbh) that were within 5 m of the transect center line were included in the sample (Fig. 2) and permanently tagged with a unique number. For each tree, species and dbh were determined. The location of each tree was mapped by recording its distance along and distance from the transect line. To assess shrub composition and biomass, a shrub plot was placed along transects every 10 m in the Shale Hills watershed and every 20 m in the Garner Run watershed. Each shrub plot $was 2m \times 2m$ (4 m^2) and centered on the transect. A smaller plot was used for measuring shrubs than for measuring trees because of the high number of shrub stems in each plot and because a microplot approach is both objective and more accurate than cover-based methods (Chojnacky and Milton 2008). A total of 318 shrub plots were used in the analysis (201 plots at Garner Run and 116 plots at Shale Hills). Within each shrub plot, all shrub stems with a diameter at root collar (DRC) between 3 mm and 10 cm were measured. For each stem, we measured DRC and identified each stem to species or genus (in the case of *Vaccinium* spp.). Only shrub species were used in biomass calculations, and young trees were excluded from the analysis (Table 1).

High-resolution lidar data were collected by the National Center for Airborne Laser Mapping (NCALM) during the leaf-on (July 2010) and leaf-off (December 2010) periods of 2010. Small footprint discrete return airborne data were acquired using an Optech Gemini ALTM 06SEN/CON195 sensor, with a scan angle of $\pm 15^{\circ}$ and an average flying height of 600 m (Lu et al. 2014). The point density was approximately 10 points $\,\mathrm{m}^{-2}$ (all returns), with a vertical accuracy of 2–4 cm. A 0.5 m resolution DEM was generated from the leaf-off flight. Root mean square error (RMSE) was not calculated on this DEM, but the average vertical error as measured from

Table 1. List of shrub species, along with citation for each species-specific equation.

Species	Author
Acer pensylvanicum	Smith and Brand 1983
Amlanchier spp.	Smith and Brand 1983
Cornus florida	Boring and Swank 1986
Crataegus spp.	Dickinson and Zenner 2010
Hamamelis virginiana	Smith and Brand 1983
Kalmia latifolia	Boring and Swank 1986
Ostrya virginiana	Means et al. 1994
Rhododendron nudiflorum	Means et al. 1994
Vaccinium spp.	Dickinson and Zenner 2010
Viburnum spp.	Dickinson and Zenner 2010

Note: References were selected based on their proximity to the study site.

flight edge matches was less than 0.05 m (NCALM 2010). Independent accuracy assessment was provided by the vendor.

2.4. Biomass calculations

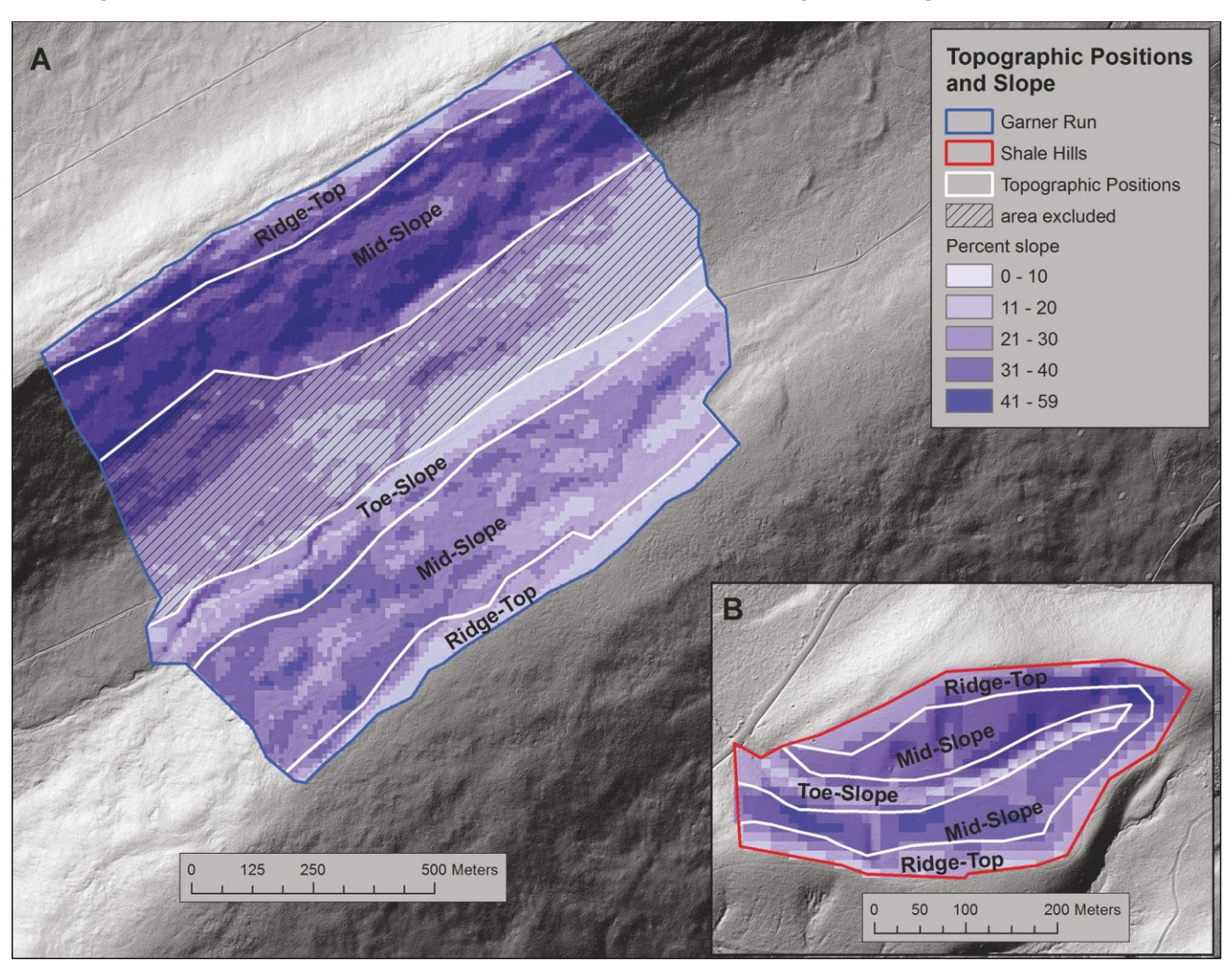
At the individual-tree level, biomass was calculated using the equations of Chojnacky et al. (2014) derived for each species group (determined by taxonomic groups and the specific gravity of wood for various species). We calculated shrub biomass using species-specific or species-group-specific allometric equations that relate DRC to biomass (Table 1; Dickinson and Zenner 2010; Smith and Brand 1983; Means et al. 1994; Boring and Swank 1986) using methods described in Chojnacky and Milton (2008).

Tree biomass was calculated for every 10 m × 10 m segment of the transect in both Shale Hills and Garner Run watersheds. For shrubs, the biomass of each stem within the 4 m² plot was calculated and summed (in tonnes (t) per hectare). Using GIS (Arc-GIS 10.3, Environmental Systems Research Institute (ESRI) 2011), the watershed was divided into toe-slope, mid-slope, and ridge-top positions to use in up-scaling the plot estimates into a watershedscale biomass estimate for each watershed. These topographic positions were identified in GIS using patterns of curvature to determine ridge-top, mid-slope, and toe-slope areas (Fig. 3). Ridgetop positions were dominated by patterns of convex curvature, mid-slope positions were areas that were dominated by planar curvature patterns, and toe-slopes dominated by concave curvature. Using the relative area of each topographic position in each watershed, a weighted mean approach was used to generate a watershed-scale tree and shrub biomass estimate for each watershed.

2.5. Effect of watershed-bedrock and topographic position on aboveground biomass in trees and shrubs

Linear mixed models were used to analyze the effect of watershed-bedrock and topographic position on aboveground biomass in trees and shrubs. Models were fitted using the "lme4" package (Bates et al. 2015) in R (R Core Team 2016). The response variable was biomass per plot for both trees and shrubs. We used a "Gaussian" error distribution for biomass. Plots nested within transect nested

Fig. 3. Ridge-top, mid-slope, and toe-slope topographic positions delineated using GIS for both (A) Garner Run and (B) Shale Hills watersheds. Percent slope at each watershed is also shown. Watersheds are not shown at the same scale. [Colour online.]



within topographic positions were included as a random effect for trees and shrubs to account for non-independence in biomass along transects.

We analyzed five models with different combinations of explanatory variables including watershed-bedrock and topographic position. Separate models were conducted for trees and shrubs. The models included a null model (intercept only), single explanatory variable models, an additive combination of the two explanatory variables, and a model with a single interaction effect. We compared the relative support of models with Akaike's information criterion (AIC; Burnham and Anderson 2002). Models were considered to have competitive support when the difference between the AIC of each model and the most supported model was <2.0 (Burnham and Anderson 2002).

2.6. Lidar analysis and processing

Lidar height metrics were calculated for both leaf-on and leaf-off lidar using the grid metrics program of FUSION (McGaughey 2009). Heights were normalized using the 0.5 m resolution lidar-derived digital elevation model (DEM) generated from the leaf-off flight. The cell size used in the grid was 10 m to correspond to the width of our vegetation sampling transects. Percent cover was calculated as the total number of first returns over a height break of 3 m, divided by the total number of first returns in the cell. We

also calculated percent cover between 0.5 m and 3 m using the cover program of FUSION (percentage of all returns occurring between heights of 0.5 m and 3 m), and the density of points that occurred between 0.5 m and 3 m using the density metrics program. These additional variables were only used as predictive variables in our shrub model.

The 1 m lidar-derived DEM was resampled using bilinear interpolation to a 10 m cell using ArcGIS 10.3 Spatial Analyst to generate terrain variables at the same scale as the vegetation data. We used the 10 m resolution DEM to generate percent slope and total curvature using the Slope and Curvature tools, respectively, in ArcGIS 10.3 Spatial Analysis extension.

2.7. Spatial model of shrub and tree biomass from leaf-on and leaf-off lidar

We used random forest regression to create a spatial model of shrub and tree biomass from leaf-on and leaf-off lidar. Random forest is an ensemble learning method used for either classification or regression. Random forest works by generating a "forest" of regression trees and randomly selects predictor variables to use in each tree. This technique has been successful with lidar data or other large datasets with many candidate variables (Cutler et al. 2007; Hudak et al. 2008; Martinuzzi et al. 2009). We chose random forest specifically because it can handle non-normally distributed

data and because it does not overfit the data, removing the need for an independent validation dataset (Breiman 2001). Because we were modeling fine-scale (10 m resolution) patterns of biomass for trees and shrubs, we chose to use a 10 m cell size for our raster-based biomass models. This is a smaller cell size than has shown to be optimal in previous lidar studies (Gobakken and Naesset 2008; Frazer et al. 2011), but because our objectives were to quantify spatial patterns of biomass across relatively small watersheds with rapidly changing terrain, we wanted to model as small of a cell size as possible. We also explored using a smaller cell size for our shrub model to match our smaller field plots but chose not to because with a smaller cell size, there were not enough lidar points getting through to the understory to get meaningful data.

Using the randomForest package (Liaw and Wiener 2002) in R (version 3.2.3, R Core Team 2016) we created a random forest regression model to predict shrub and tree biomass separately. We modeled both watersheds simultaneously in the same model. Variables for leaf-on and leaf-off height grid metrics, as well as previously described terrain variables, were assessed for importance to initially build models for tree and shrub biomass (Table 2). We included UTM eastings and northings to assess whether adding spatial data would improve model performance (Mascaro et al. 2014). Additionally, a variable measuring the distance between the center of the measured plot on the ground and the center of the grid cell was included to determine if this distance had an effect on the model results. Leaf-on and leaf-off lidar variables were modeled separately and then combined to fully explore the effectiveness of leaf-on and leaf-off lidar in our study site. In randomForest, the importance of variables is assessed using %IncMSE, which shows the percent increase of mean squared error (MSE) if the variable was randomly shuffled in the model. To determine which variables were important and to ensure a parsimonious model, variables in the final model were chosen using an iterative process whereby variables that had low importance values (%IncMSE) were removed systematically until we were able to build a model that maximized the amount of variance explained (Díaz-Uriarte and Alvarez de Andrés 2006). Additionally, in the case of highly intercorrelated variables (Pearson > 0.75), the variable that was less important (from %IncMSE) was removed from consideration. We assessed the accuracy of our final model by analyzing the percent variance explained, which is a pseudo R^2 . We also validated the model by applying the model to a separate set of plots that were not used to generate the model. We calculated RMSE and relative RMSE using the independent validation dataset, based on modeled versus actual biomass values for the validation plots.

Along each 100 m segment of the transect, three 200 m² plots (20m× 10 m) were identified and used as ground plots on which to fit our tree biomass model, and one 200 m² plot was used as a validation plot. We spaced these along each segment to avoid overlap within single lidar grid cells and used a 20 m length (vs. 10 m length used for biomass calculations from field data) to account for possible location errors associated with either GPS or a misalignment of cells between the raster and the ground plot. Both Frazer et al. (2011) and Gobakken and Naesset (2008) note that with a larger ground plot size, there is less of an effect from GPS positioning errors. Also, using a slightly larger ground plot reduces error caused by edge effect (trees with stems outside of the plot and portions of their canopy inside the plot) (Frazer et al. 2011). Although it has previously been suggested that raster cell size should match the size of the ground plots used to calibrate the model (White et al. 2013), optimal ground plot size does not necessarily align with the cell size from lidar-based metrics (Hayashi et al. 2015) Additionally, it may be beneficial to map forest attributes at a higher precision than the plot size, particularly with a high-density lidar dataset (Silva et al. 2017). A total of 167 plots were used to fit the model, and 54 plots were used for validation.

To build the model for shrub biomass, the same process was used, with the addition of the percent low cover and 3 m density variables for both leaf-on and leaf-off lidar. Two-hundred and fifty-three shrub plots were used to fit the model, and 63 randomly chosen plots were used during the model validation process.

Once random forest models were created that explained the maximum amount of variance for both tree biomass and shrub biomass, these models were applied to the rest of the watershed using a $10\,\mathrm{m}\times10\,\mathrm{m}$ grid. Mean biomass values from the raster model for trees and shrubs were compared with mean measured biomass values for each topographic position.

3. Results

3.1. Biomass values across topographic position and watershed

For both watersheds, the toe-slope position had the greatest biomass (Table 3). At Shale Hills, the ridge-top position had the lowest biomass, while at Garner Run, the mid-slope position on the southern aspect had the lowest biomass (Table 3). Using weighted means for each topographic position, excluding the recently harvested area, the average biomass of trees was 247.43 t·ha⁻¹ with a standard deviation of 73.6 t·ha⁻¹ in Shale Hills and 155.20 t·ha⁻¹ with a standard deviation of 41.5 t·ha⁻¹ at Garner Run. The greatest proportion of biomass in trees was stored in *Quercus* spp. at both Shale Hills and Garner Run.

Shrub biomass was considerably less than tree biomass (<1% at most locations) (Table 3). The shrub biomass at Shale Hills was less than 20% of the mean shrub biomass at Garner Run. Biomass of the understory vegetation was highest at the ridge-top position at both watersheds. Understory vegetation at Garner Run, dominated by *Kalmia latifolia* and *Vaccinium* spp., was denser and represented a greater proportion of the total aboveground biomass than Shale Hills.

3.2. Mixed models results of biomass per watershed and topographic position

The most supported model for aboveground biomass in trees and shrubs included watershed-bedrock and topographic position and the interaction between these two variables (Table 4). Additive models without the interaction term also explained shrub biomass variation (LAIC = 0.50), but they did not perform as well for tree biomass variation (LAIC = 33.91).

3.3. Random forest model for tree and shrub biomass using leaf-on and leaf-off lidar

We tested 30 leaf-on and 30 leaf-off lidar variables, five terrain variables, and three location variables for our random forest model of tree biomass (Table 2). Results of best performing leafon, leaf-off, and combined models are shown in Table 5. Leaf-off data on its own explained more variance in biomass than leaf-on data, and by using combined leaf-on and leaf-off data, we developed a model with six variables that explained 48% of the variance (pseudo R^2) of tree biomass, with the most important variables being 60th percentile height and elevation (Fig. 4). Using the independent validation dataset, RMSE of the tree biomass model was 87.9 t·ha-1, and relative RMSE was 0.44. Patterns of error show that, generally, the model is smoothing out variability of the biomass values, and for lower biomass values, the random forest model is overpredicting biomass, while at higher biomass values, the model is underpredicting biomass (Fig. 5). In general, modeled biomass values are closer to the mean than measured biomass

We tested 32 leaf-on and 32 leaf-off lidar variables, five terrain variables, and three location variables in our model of shrub biomass (Table 2). Results of best performing leaf-on, leaf-off, and combined models are shown in Table 5. Unlike our lidar-based tree model, leaf-on data explained much more variance than leaf-off data in our shrub biomass model. Using combined leaf-on and

Table 2. Candidate and selected variables used in the random forest models for shrub and tree biomass using both leaf-on and leaf-off variables separately and combined.

		Tree biomass		Shrub biomass			
Variable name	Variable description	Leaf-on	Leaf-off	Leaf-on	Leaf-off	Tree biomass combined	Shrub biomass combined
Lidar elevation							
lon_returnct	Leaf-on total return count						
loff_returnct	Leaf-off total return count						
lon_min	Leaf-on elevation minimum (m)						
loff_min	Leaf-off elevation minimum (m)				×		
lon_max	Leaf-on elevation maximum (m)						
loff_max	Leaf-off elevation maximum (m)						
lon_mean	Leaf-on elevation mean (m)	×					
loff_mean lon mode	Leaf-off elevation mean (m) Leaf-on elevation mode (m)		×	×		×	×
loff_mode	Leaf-off elevation mode (m)			^			^
lon_stdev	Leaf-on elevation standard deviation						
loff_stdev	Leaf-off elevation standard deviation						
lon_var	Leaf-on elevation variance						
loff_var	Leaf-off elevation variance						
lon_cv	Leaf-on coefficient of variation						
loff_cv	Leaf-off coefficient of variation						
lon_iq	Leaf-on elevation interquartile						
loff_iq	Leaf-off elevation interquartile						
lon_skewn loff_skewn	Leaf-on elevation skewness Leaf-off elevation skewness				×		
lon_kurto	Leaf-on elevation kurtosis			×	^		×
loff kurto	Leaf-off elevation kurtosis			^	×		^
lon_ADD	Leaf-on average absolute deviation						
loff_ADD	Leaf-off average absolute deviation						
lon_p01	Leaf-on 1st percentile height						
loff_p01	Leaf-off 1st percentile height						
lon_p05	Leaf-on 5th percentile height						
loff_p05	Leaf-off 5th percentile height						
lon_p10	Leaf-on 10th percentile height			×			×
loff_p10 lon_p20	Leaf-off 10th percentile height Leaf-on 20th percentile height						
loff_p20	Leaf-off 20th percentile height						
lon_p25	Leaf-on 25th percentile height			×			×
loff_p25	Leaf-off 25th percentile height						
lon_p30	Leaf-on 30th percentile height					×	
loff_p30	Leaf-off 30th percentile height		×		×		
lon_p40	Leaf-on 40th percentile height	×					
loff_p40	Leaf-off 40th percentile height						
lon_p50	Leaf-on 50th percentile height						
loff_p50	Leaf-off 50th percentile height Leaf-on 60th percentile height						
lon_p60 loff_p60	Leaf-off 60th percentile height	×				×	
lon_p70	Leaf-on 70th percentile height						
loff_p70	Leaf-off 70th percentile height						
lon_p75	Leaf-on 75th percentile height						
loff_p75	Leaf-off 75th percentile height						
lon_p80	Leaf-on 80th percentile height						
loff_p80	Leaf-off 80th percentile height						
lon_p90	Leaf-on 90th percentile height						
loff_p90 lon_p95	Leaf-off 90th percentile height Leaf-on 95th percentile height		×			×	
loff_p95	Leaf-off 95th percentile height						
lon_p99	Leaf-on 99th percentile height	×		×			×
loff_p99	Leaf-off 99th percentile height		×		×		
lon_cover	Leaf-on cover height break of 3 m						
loff_cover	Leaf-off cover height break of 3 m				×		
lon_cover1	Leaf-on cover first return only			×			×
loff_cover1	Leaf-off cover first return only		×			×	
lon_can_rel	Leaf-on canopy relief ratio						
loff_can_rel	Leaf-off canopy relief ratio				×		
lon_dens3 loff_dens3	Leaf-on density between 0.25 and 3 m Leaf-off density between 0.25 and 3 m						

Table 2 (concluded).

		Tree biomass		Shrub biomass			
Variable name	Variable description	Leaf-on	Leaf-off	Leaf-on	Leaf-off	Tree biomass combined	Shrub biomass combined
lon_cover3 loff_cover3	Leaf-on cover between 0.25 and 3 m Leaf-off cover between 0.25 and 3 m						
Terrain perc_slope elev curv aspdeg watershed x_coor y_coord	Percent slope at 10 m resolution Elevation (m) Combined curvature at 10 m cell Aspect in degrees Sandstone or shale watershed UTM easting UTM northing		×	× ×	×	×	× ×

Table 3. Mean values for field-measured and random forest modeled shrub and tree biomass values for each topographic position in Shale Hills and Garner Run watersheds.

Topographic position	Field-measured tree biomass (t·ha ⁻¹)	Random forest modeled tree biomass (t·ha ⁻¹)	Field-measured shrub biomass (t·ha ⁻¹)	Random forest modeled shrub biomass (t·ha ⁻¹)
Shale Hills				
Ridge-top	174.2 (55.8) ^a	198.9	$0.6 (0.6)^a$	1.0
Mid-slope	284.6 (54.7)	244.5	0.3 (0.6)	0.6
Toe-slope	305.1 (40.5)	310.2	0.1 (0.1)	0.3
Garner Run				
Ridge-top	160.3 (24.1)	151.4	3.3 (3.9)	2.3
Mid-slope northern aspect	172.6 (32.0)	162.4	1.7 (2.6)	1.4
Mid-slope southern aspect	121.1 (39.2)	126.0	1.4 (2.2)	2.0
Toe-slope	191.4 (45.2)	210.2	1.3 (1.3)	1.5

aStandard deviation in parentheses.

Table 4. Model selection statistics for tree and shrub biomass mixed models.

Model	LAIC	W_i	1	K
Tree biomass				
$T + W + T \times W$	0.00	1.00	-5812.46	9
T + W	33.91	0.00	-5831.42	7
W	36.68	0.00	-5834.80	5
T	124.06	0.00	-5877.49	6
I	231.03	0.00	-5932.98	4
Shrub biomass				
$T + W + T \times W$	0.00	0.54	-2280.05	9
T + W	0.50	0.34	-2282.30	7
W	5.79	0.03	-2286.94	5
T	29.64	0.00	-2297.87	6
I	31.75	0.00	-2300.92	4

Note: Main effects include topographic position (T) and watershedbedrock (W). The null model is represented by I (intercept only). Summary includes relative difference between model AIC and AIC for the best model (LAIC), Akaike weights (w_i) , log-likelihood (I), and number of parameters (K).

leaf-off data, we developed a model with eight variables that explained 24% of the variance (pseudo R^2). Using the independent validation dataset, RMSE of the shrub biomass model was 1.3 t·ha⁻¹, and relative RMSE was 1.2. All of the important variables were leaf-on or terrain variables, with the two most important variables being elevation and 10th percentile height (Fig. 4). The patterns of errors for shrub biomass are similar to those of trees, with lower biomass values being overpredicted and higher biomass values being underpredicted. In particular, there are a lot of plots with a measured shrub biomass of zero and not many modeled plots with a value of zero (Fig. 5). Again, the model is smoothing the biomass values, and predicted values are consistently closer to the average biomass than measured biomass plots.

3.4. Spatial patterns of random forest modeled tree and shrub biomass

Random forest modeled tree biomass values were higher on the Shale Hills watershed than on the Garner Run watershed (Figs. 6A and 6B). In both watersheds, higher biomass was found along the valley bottom, with lower values for the ridge-top (Table 3). At Shale Hills, higher biomass values occur up to the midpoint of the hillslope and on the north-facing slope of the watershed (Fig. 6B). At Garner Run, biomass is lower and there is more variability within adjacent pixels at all topographic positions (Fig. 6A). Although modeled biomass values are higher in the valley bottom and lower in the mid-slope and ridge-top, the values decrease quickly above the toe-slope on the northern aspect.

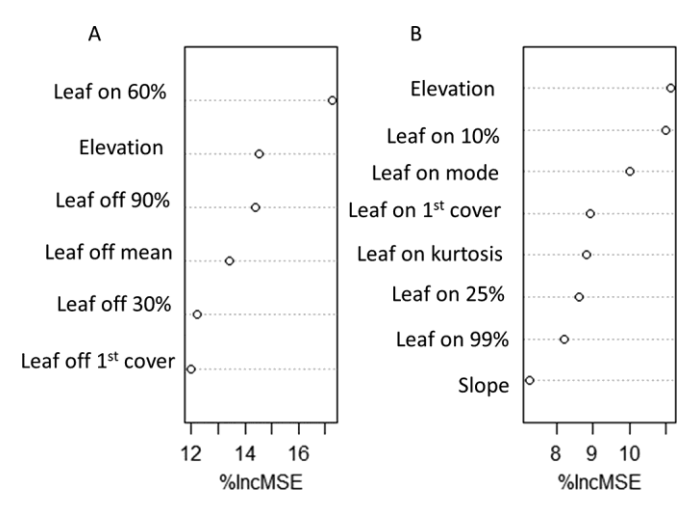
Random forest modeled shrub biomass was higher on Garner Run than on Shale Hills, and the spatial patterns of modeled shrub biomass were different for each watershed (Figs. 6C and 6D). At Shale Hills, biomass values for shrubs were low across the entire watershed but were slightly higher on the ridge-top. Near the stream and across much of the watershed, the values were either zero or close to zero. There is a clear ring around the top edge of the watershed boundary with higher biomass values and a moderate amount of variability (Fig. 6D).

At the Garner Run watershed, a different pattern emerged in which high biomass values were found at the ridge-top but with a secondary peak found adjacent to the stream in the toe-slope position, likely due to the presence of *Rhododendron maximum* (Fig. 6C). In general, shrub biomass was variable across the watershed, but the ridge-tops, as well as the southern aspect mid-slope and the upstream end of the watershed, had consistently high values. The mid-slope positions were highly variable but tended to have lower biomass values overall. Even though the model for shrub biomass had a lot of unexplained variation, the trends of shrub biomass match those observed in the field measurements (Table 3).

Table 5. Number of variables and percent variance explained (pseudo R^2) of random forest models of biomass
derived from leaf-off lidar only, leaf-on lidar only, and combined leaf-off and leaf-on lidar.

	Tree biomass		Shrub biomass			
Model component	Leaf-on	Leaf-off	Leaf-on	Leaf-off	Tree biomass combined	Shrub biomass combined
No. of variables	4	6	8	8	6	8
% Variance explained	40	45	24	8	48	24

Fig. 4. Percent increase of mean standard error (MSE) for each variable in the final random forest model for (A) trees and (B) shrubs. %IncMSE shows the percent increase of MSE if the variable was randomly shuffled in the model.



4. Discussion

This study highlights the range of variability of biomass and forest structure within similar forest communities. Both modeled and field-measured estimates of biomass showed $\sim\!60\%$ greater biomass in Shale Hills compared with Garner Run, despite their relative proximity and similar oak-dominated deciduous forest cover. Within watersheds, forest biomass was generally highest at the toe-slope position and decreased moving to the mid-slope and then to the ridge-top. The greatest proportion of forest biomass is found in trees ($\sim\!99\%$), but the relatively small amount of shrub biomass (remaining $\sim\!1\%$) can provide important ecosystem services such as wildlife habitat, therefore accurate models of shrub biomass can be equally useful for managers.

We also improved our understanding as to how leaf-on and leaf-off lidar can be used for modeling patterns of tree and shrub biomass across broad scales. Collecting field data for biomass estimates is time consuming and costly and usually includes only a fraction of the landscape. Both leaf-on and leaf-off lidar data were essential for characterizing biomass from trees and shrubs in a deciduous forest. Leaf-off lidar was more effective at characterizing tree biomass, while leaf-on lidar was more effective at characterizing shrub biomass.

4.1. Biomass values across watersheds and topographic position

Topographic position, watershed, and the interaction of those variables influenced the biomass of both trees and shrubs. The interaction effect, in particular, suggests that the biomass may not be responding to the same factors in each watershed. Differences in bedrock, soil, and elevation in watersheds contribute to vegetation changes and forest height, which can directly influence biomass (Wolf et al. 2016; Bolstad et al. 2018). This could be due in part to the influence of bedrock on landscape evolution. For example, hillslope length at Garner Run is much longer than

Shale Hills due perhaps to slower erosion for sandstone than shale (Brantley et al. 2016). At the Shale Hills watershed, in addition to the concave area near the stream and toe-slope, there are also dominant swale features that intersect the mid-slope area. Swales host higher forest productivity than planar slopes in Shale Hills (Smith et al. 2017) and may contribute to higher biomass in the overall watershed compared with Garner Run. Swales and a stream basin are not present in the Garner Run watershed, and the hillslope is more planar. The difference that we see in biomass distributions between topographic positions and watersheds could be caused by topography-driven patterns in soil depth and water availability, as well as differences in nutrient availability between bedrock (Hahm et al. 2014).

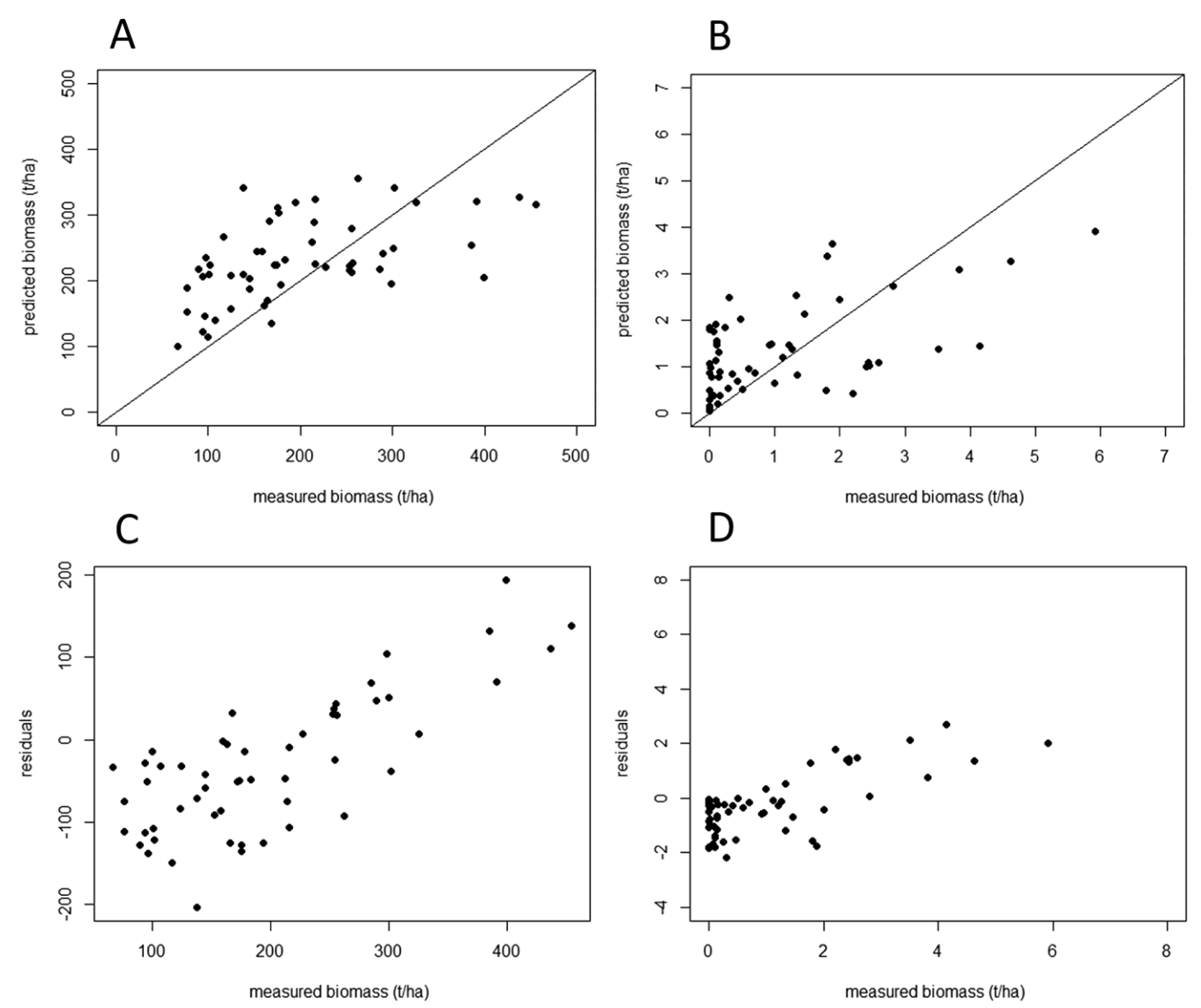
4.2. Leaf-on and leaf-off lidar models

One of the advances made in this study is understanding how leaf-on and leaf-off data can be used together to represent forest structure, particularly with a complex canopy structure and the presence of important understory species. Although others (Hill and Broughton 2009) have suggested that leaf-off data could be more effective at identifying understory or complex canopies, we did not find that to be the case for understory biomass. In our shrub biomass model, leaf-on variables were much more important than leaf-off variables, which contradicts the idea that in leafoff conditions, more lidar points would penetrate the canopy and reach the shrub layer. With fewer leaves on the shrubs, there were not enough lidar points from the understory to accurately reflect shrub biomass. Our results are consistent with studies done in tropical forests in which leaf-on data were found to be more effective at modeling biomass and biodiversity (García et al. 2010).

Our results investigating the role of leaf-on and leaf-off lidar data to model tree biomass showed that leaf-off lidar data modeled tree biomass slightly more effectively than leaf-on data. In this closed deciduous forest ecosystem, the leaf-on lidar percent cover seems to be oversaturated with respect to biomass, meaning that there is not much variability in leaf-on percent cover (most values are close to 100%), although there is variability in biomass. There is less two-dimensional variability in canopy cover than in biomass. This may be because when a tree dies, the trees around it will spread their canopy to fill in the gap, with potentially little influence on biomass estimates based on tree diameter. With leafoff lidar data, differences in percent cover are slightly more pronounced, as evidenced by the leaf-off first return cover being included in the final leaf-off lidar tree biomass model. Therefore, leaf-off lidar is slightly better at detecting subtle differences in forest density that relates to biomass than leaf-on lidar in this deciduous forest.

Our models of tree biomass did not predict biomass as well as other lidar studies investigating deciduous or mixed forests (Gleason and Im 2012; Wolf et al. 2016), perhaps in part because of our small plot and raster cell size. Optimal plot and cell size has been extensively researched with respect to lidar-based measurements (Gobakken and Naesset 2008; Frazer et al. 2011; White et al. 2013; Ruiz-Benito et al. 2014; Hayashi et al. 2016; Silva et al. 2017), but results vary based on lidar pulse density and forest structure. Hayashi et al. (2016) and Silva et al. (2017) both found that a 10 m resolution raster-based model may effectively model biomass, but

Fig. 5. The measured versus modeled biomass values for (A) trees and (B) shrubs using the random forest model for the validation points. The total variance (pseudo R^2) explained by the random forest models for tree and shrub biomass were 48% and 24%, respectively. Patterns of residuals with respect to measured biomass are shown in (C) trees and (D) shrubs.



in our case, this cell size seems to have been smaller than optimal. Our objective was to develop a model that would highlight fine-scale patterns, but in increasing the spatial resolution of our models, we probably also increased the amount of unexplained variability in our model. With a small plot size, the presence or absence of one tree can have a significant impact on the total biomass value for the plot. Also, a tree that has its canopy inside the plot, as measured by the lidar, may have a stem outside of the plot; therefore, its biomass would not be included in our field measurement.

In a model of shrub abundance, Barber et al. (2016) used a variable measuring the percentage of returns higher than 1.37 m, as well as a variable measuring the percentage of first returns between 0.15 m and 1.37 m. Using models with only lidar data, they were able to explain between about 14% and 24% of the variability in abundance for two different shrub species, which compares with our models, which explained about 24% of the shrub biomass variability. In modeling understory biomass, we considered the approach of Hudak et al. (2016) that used only lidar returns between 0 and 3 m to calculate shrub biomass and then used over-

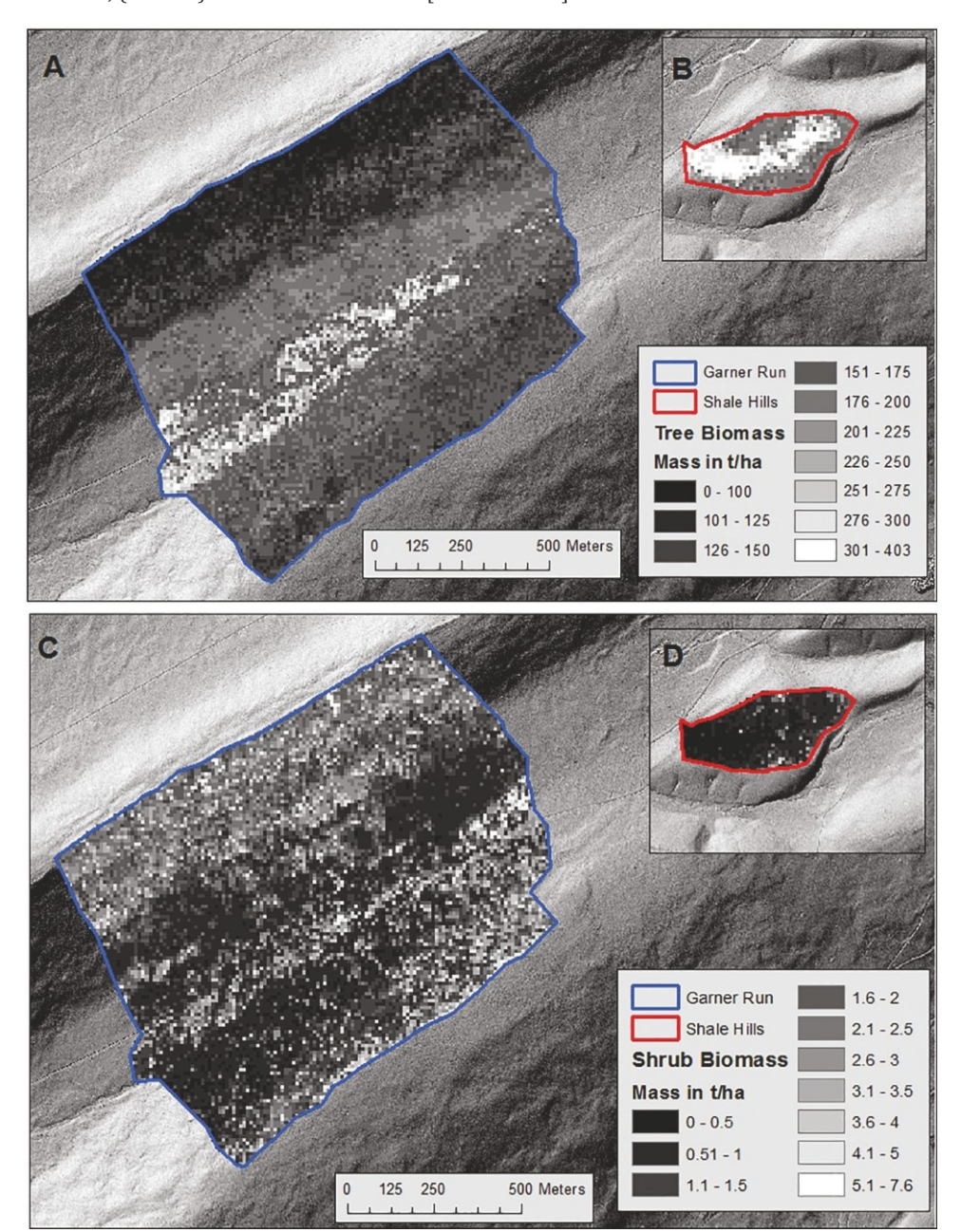
story canopy cover as a correction factor. Unfortunately, we found that in many cases, we did not have enough returns in the understory layer, particularly in the leaf-off lidar dataset, to generate accurate models of shrubs. Hill and Broughton (2009) calculated height of understory using leaf-off and leaf-on lidar by measuring the height of the highest return below the canopy. We were interested in the biomass from shrubs, which is affected more by stem density than height, so we chose to use the entire point cloud for our models.

We found similar lidar metrics to be important for modeling tree biomass, as in other studies (e.g., Wolf et al. 2016; Gleason and Im 2012; Hudak et al. 2012). In our tree biomass model, leaf-on 60% percentile height was the most important metric. Also, elevation was the only important terrain metric for the tree biomass model. Other terrain metrics may not have been important because the different watersheds have different bedrock and, subsequently, their patterns of landscape evolution are different.

4.3. Spatial patterns of biomass

Across topographic positions, shrub biomass was consistently higher in the Garner Run watershed than in the Shale Hills water-

Fig. 6. Random forest modeled values of tree and shrub biomass (in $t \cdot ha^{-1}$) for both (A, C) Garner Run and (B, D) Shale Hills watersheds: (A and B) tree biomass models; (C and D) shrub biomass models. [Colour online.]



shed. Because we analyzed only two watersheds for this study, we are unable to predict why this may be occurring, but in other areas, forest structure varies with bedrock type (Butler et al. 2003; Hahm et al. 2014). In this region, sandstone frequently underlays dry oak–heath forests, which are characterized by an ericaceous shrub understory (Fike 1999). The developed shrub understory may be the result of higher soil acidity and (or) lower water availability associated with sandstone-derived soils. Future work will expand the scope of this study to determine if this is a consistent pattern for eastern deciduous forests across bedrock types.

The patterns of shrub biomass and tree biomass across the watersheds tend to be opposite to one another, with shrub biomass values being higher on ridge-tops and tree biomass values being higher in toe-slope positions, with some exceptions. Previous lidar research has shown that shrub biomass tends to vary inversely

with tree canopy cover (Martinuzzi et al. 2009; Bolstad et al. 2018). Although our overall biomass results for trees and shrubs by topographic position support this idea, the lidar-derived percent tree cover metric was not one of the important variables in our shrub biomass models, showing that there is not a direct inverse relationship between percent tree cover and shrub biomass. This may be because in this ecosystem, the lidar signal for percent cover may be saturated at a relatively low level of tree biomass, thereby making it a less effective predictor of light availability for understory than it may be in other forest types. Another contradiction is that at the toe-slope of the Garner Run watershed, the shrub biomass values are actually relatively high, despite the fact that tree biomass is also high. We think that this may be because of some large understory species (e.g., Rhododendron maximum and Hamamelis virginiana L.) that primarily occur along the stream in this watershed.

4.4. Study limitations and sources of error

There are several limitations of our sampling scheme for answering questions about patterns of biomass. First, we did not have replicates for each watershed; therefore, it is unclear if the patterns in tree and shrub biomass across watersheds would be consistent based on bedrock. Second, our field plot size is small compared with other studies, particularly our shrub plots, which could lead to increased error in the lidar-based biomass models. We were also relying on current GPS technology, which makes it difficult to perfectly line up high-resolution lidar to relatively small plots on the ground.

Another source of error in our study is the allometric equations used to relate diameter to tree biomass. Smith et al. (2017) estimated 10% uncertainty in their biomass calculations from tree diameters for Shale Hills due to field measurement and model selection uncertainty. Lidar-based metrics are often based on tree height, while the allometric equations used to calculate biomass from field measurements are based on tree diameter. Trees of the same species and diameter were consistently taller in Shale Hills than in Garner Run, and trees were taller at the toe-slope position than at the ridge-top position. Although our biomass values, both measured and modeled, were consistently higher at the toe-slope position and at the Shale Hills watershed, these differences are probably underestimated because biomass estimates do not take into account tree height and, therefore, cannot capture the effects of topographic position and watershed on tree biomass via tree height.

5. Conclusions

The major objective of this study was to understand how aboveground biomass varies with changing terrain at a fine-scale (10 m) resolution. We found a much higher amount of shrub biomass in the Garner Run watershed than in the Shale Hills watershed at all topographic positions. Within each watershed, there was higher tree biomass at the toe-slope position, and shrub biomass values varied across topographic position for each watershed. This suggests that there are other abiotic factors in addition to topography that influence the distribution of biomass across the landscape.

We also used leaf-on and leaf-off lidar for modeling shrub and tree biomass. We were able to model broad-scale patterns of biomass using both leaf-on and leaf-off lidar, but our most accurate model is not capturing the full range of variability on a fine scale. Because shrub biomass in particular is difficult to measure in the field, a stratified sampling method could be employed in the future to capture more of the variability in high shrub areas such as in ridge-top topographic positions, which could lead to improved spatial models. Overall, by understanding how biomass varies spatially at a fine scale, we can begin to link ecosystem processes to abiotic factors and optimize ecosystem services at a landscape scale.

Acknowledgements

This work was supported by NSF Critical Zone Observatory program grants to C. Duffy (EAR 07-25019) and S. Brantley (EAR 12-39285, EAR 13-31726). This research was conducted partially in Penn State's Stone Valley Forest, which is supported and managed by the Penn State's Forestland Management Office in the College of Agricultural Sciences. Research was also conducted in the Rothrock State Forest, managed by Pennsylvania DCNR Bureau of Forestry. Fieldwork was conducted by students in the CZO REU program, as well as Chad Tokowicz, Russell Symmes, and Katharine Boeding. The authors thank Elizabeth Newell for providing feedback on an earlier draft and Laura Leites and Bradley Cosentino for providing analysis advice. The authors also thank anonymous reviewers for their feedback.

References

- Asner, G.P., Knapp, D.E., Kennedy-Bowdoin, T., Jones, M.O., Martin, R.E., Boardman, J., and Hughes, R.F. 2008. Invasive species detection in Hawaiian rainforests using airborne imaging spectroscopy and LiDAR. Remote Sens. Environ. 112: 1942–1955. doi:10.1016/j.rse.2007.11.016.
- Asner, G.P., Mascaro, J., Muller-Landau, H.C., Vieilledent, G., Vaudry, R., Rasamoelina, M., Hall, J.S., and van Breugel, M. 2012. A universal airborne LiDAR approach for tropical forest carbon mapping. Oecologia, **168**: 1147–1160. doi:10.1007/s00442-011-2165-z. PMID:22033763.
- Barber, Q.E., Bater, C.W., Braid, A.C., Coops, N.C., Tompalski, P., and Nielsen, S.E. 2016. Airborne laser scanning for modelling understory shrub abundance and productivity. For. Ecol. Manage. 377: 46–54. doi:10.1016/j.foreco.2016.06. 037
- Bates, D., Kliegl, R., Vasishth, S., and Baayen, H. 2015. Parsimonious mixed models. arXiv:1506.04967.
- Birdsey, R.A. 1992. Carbon storage and accumulation in United States forest ecosystems. USDA Forest Service, Washington Office, Washington, D.C., Gen. Tech. Rep. WO-59. doi:10.2737/WO-GTR-59.
- Bolstad, P.V., Swank, W., and Vose, J. 1998. Predicting Southern Appalachian overstory vegetation with digital terrain data. Landscape Ecol. 13: 271–283. doi:10.1023/A:1008060508762.
- Bolstad, P.V., Elliott, K.J., and Miniat, C.F. 2018. Forests, shrubs, and terrain: top-down and bottom-up controls on forest structure. Ecosphere, 9: e02185. doi:10.1002/ecs2.2185.
- Boring, L.R., and Swank, W.T. 1986. Hardwood biomass and net primary production following clearcutting in the Coweeta Basin. *In* Proceedings of the 1986 Southern Forest Biomass Workshop, Knoxville, Tenn., 16–19 June 1986. Tennessee Valley Authority, Norris, Tenn. pp. 43–50.
- Brandtberg, T., Warner, T.A., Landenberger, R.E., and McGraw, J.B. 2003. Detection and analysis of individual leaf-off tree crowns in small footprint, high sampling density LiDAR data from the eastern deciduous forest in North America. Remote Sens. Environ. 85: 290–303. doi:10.1016/S0034-4257f03100008-7.
- Brantley, S.L., DiBiase, R.A., Russo, T.A., Shi, Y., Lin, H., Davis, K.J., Kaye, M., Hill, L., Kaye, J., Eissenstat, D.M., Hoagland, B., Dere, A.L., Neal, A.L., Brubaker, K.M., and Arthur, D.K. 2016. Designing a suite of measurements to understand the critical zone. Earth Surf. Dyn. 4: 211–235. doi:10.5194/esurf-4-211-2016.
- Brantley, S.L., Eissenstat, D.M., Marshall, J.A., Godsey, S.E., Balogh-Brunstad, Z., Karwan, D.L., Papuga, S.A., Roering, J., Dawson, T.E., Evaristo, J., Chadwick, O., McDonnell, J.J., and Weathers, K.C. 2017. Reviews and syntheses: on the roles trees play in building and plumbing the critical zone. Biogeosciences, 14: 5115–5142. doi:10.5194/bg-14-5115-2017.
- Breiman, L. 2001. Random forests. Mach. Learn. 45: 5-32. doi:10.1023/A: 1010933404324.
- Brose, P.H. 2016. Origin, development, and impact of mountain laurel thickets on the mixed-oak forests of the central Appalachian Mountains, USA. For. Ecol. Manage. 374: 33–41. doi:10.1016/j.foreco.2016.04.040.
- Brown, S.L., Schroeder, P., and Kern, J.S. 1999. Spatial distribution of biomass in forests of the eastern USA. For. Ecol. Manage. 123: 81–90. doi:10.1016/S0378-1127(99)00017-1.
- Brubaker, K.M., Johnson, S.E., Brinks, J., and Leites, L.P. 2014. Estimating canopy height of deciduous forests at a regional scale with leaf-off, low point density LiDAR. Can. J. Remote Sens. 40: 123–134.
- Burnham, K.P., and Anderson, D.R. 2002. Model selection and multimodel inference: a practical information-theoretic approach. Springer-Verlag, New York. doi:10.1007/b97636.
- Butler, D.R., Malanson, G.P., Bekker, M.F., and Resler, L.M. 2003. Lithologic, structural, and geomorphic controls on ribbon forest patterns in a glaciated mountain environment. Geomorphology, 55: 203–217. doi:10.1016/S0169-555X(03)00140-5.
- Chance, C.M., Coops, N.C., Crosby, K., and Aven, N. 2016. Spectral wavelength selection and detection of two invasive plant species in an urban area. Can. J. Remote Sens. 42: 27–40. doi:10.1080/07038992.2016.1143330.
- Chojnacky, D.C., and Milton, M. 2008. Measuring carbon in shrubs. *In* Field measurements for forest carbon monitoring: a landscape-scale approach. *Edited by* C.M. Hoover. Springer, Dordrecht, Netherlands. pp. 45–72. doi:10. 1007/978-1-4020-8506-2_5.
- Chojnacky, D.C., Heath, L.S., and Jenkins, J.C. 2014. Updated generalized biomass equations for North American tree species. Forestry, 87: 129–151. doi:10.1093/ forestry/cpt053.
- Ciolkosz, E.J., Waltman, W.J., Simpson, T.W., and Dobos, R.R. 1989. Distribution and genesis of soils of the northeastern United States. Geomorphology, 2: 285–302. doi:10.1016/0169-555X(89)90016-0.
- Curtis, P.S. 2008. Estimating aboveground carbon in live and standing dead trees. *In* Field measurements for forest carbon monitoring: a landscape-scale approach. *Edited by* C.M. Hoover. Springer, Dordrecht, Netherlands. pp. 39–44. doi:10.1007/978-1-4020-8506-2_4.
- Cutler, D.R., Edwards, T.C., Beard, K.H., Cutler, A., Hess, K.T., Gibson, J., and Lawler, J.J. 2007. Random forests for classification in ecology. Ecology, 88: 2783–2792. doi:10.1890/07-0539.1. PMID:18051647.
- de Castilho, C.V., Magnusson, W.E., de Araújo, R.N.O., Luizão, R.C.C., Luizão, F.J., Lima, A.P., and Higuchi, N. 2006. Variation in aboveground tree live biomass

in a central Amazonian Forest: effects of soil and topography. For. Ecol. Manage. **234**: 85–96. doi:10.1016/j.foreco.2006.06.024.

- Defibaugh y Chávez, J., and Tullis, J.A. 2013. Deciduous forest structure estimated with LiDAR-optimized spectral remote sensing. Remote Sens. 5: 155–182. doi:10.3390/rs5010155.
- Díaz-Uriarte, R., and Alvarez de Andrés, S. 2006. Gene selection and classification of microarray data using random forest. BMC Bioinf. 7: 3. doi:10.1186/1471-2105-7-3.
- Dickinson, Y.L., and Zenner, E.K. 2010. Allometric equations for the aboveground biomass of selected common eastern hardwood understory species. North. J. Appl. For. 27: 160–165.
- Duncanson, L.I., Dubayah, R.O., and Enquist, B.J. 2015. Assessing the general patterns of forest structure: quantifying tree and forest allometric scaling relationships in the United States. Global Ecol. Biogeogr. 24: 1465–1475. doi: 10.1111/geb.12371.
- Environmental Systems Research Institute (ESRI). 2011. ArcGIS Desktop. Release 10. Environmental Systems Research Institute, Redlands, Calif.
- Fedrigo, M., Newnham, G.J., Coops, N.C., Culvenor, D.S., Bolton, D.K., and Nitschke, C.R. 2018. Predicting temperate forest stand types using only structural profiles from discrete return airborne lidar. ISPRS J. Photogramm. Remote Sens. 136: 106–119. doi:10.1016/j.isprsjprs.2017.11.018.
- Fike, J. 1999. Terrestrial and palustrine plant communities of Pennsylvania. Pennsylvania Natural Diversity Inventory, Harrisburg, Penn.
- Frazer, G.W., Magnussen, S., Wulder, M.A., and Niemann, K.O. 2011. Simulated impact of sample plot size and co-registration error on the accuracy and uncertainty of LiDAR-derived estimates of forest stand biomass. Remote Sens. Environ. **115**: 636–649. doi:10.1016/j.rse.2010.10.008.
- García, M., Riaño, D., Chuvieco, E., and Danson, F.M. 2010. Estimating biomass carbon stocks for a Mediterranean forest in central Spain using LiDAR height and intensity data. Remote Sens. Environ. 114: 816–830. doi:10.1016/j.rse.2009. 11.021.
- Gleason, C.J., and Im, J. 2012. Forest biomass estimation from airborne LiDAR data using machine learning approaches. Remote Sens. Environ. 125: 80–91. doi:10.1016/j.rse.2012.07.006.
- Gobakken, T., and Næsset, E. 2008. Assessing effects of laser point density, ground sampling intensity, and field sample plot size on biophysical stand properties derived from airborne laser scanner data. Can. J. For. Res. 38(5): 1095–1109. doi:10.1139/X07-219.
- Gopalakrishnan, R., Thomas, V.A., Wynne, R.H., Coulston, J.W., and Fox, T.R. 2018. Shrub detection using disparate airborne laser scanning acquisitions over varied forest cover types. Int. J. Remote Sens. 39: 1220–1242. doi:10.1080/01431161.2017.1399476.
- Greaves, H.E., Vierling, L.A., Eitel, J.U., Boelman, N.T., Magney, T.S., Prager, C.M., and Griffin, K.L. 2015. Estimating aboveground biomass and leaf area of low-stature Arctic shrubs with terrestrial LiDAR. Remote Sens. Environ. **164**: 26–35. doi:10.1016/j.rse.2015.02.023.
- Hahm, W.J., Riebe, C.S., Lukens, C.E., and Araki, S. 2014. Bedrock composition regulates mountain ecosystems and landscape evolution. Proc. Natl. Acad. Sci. 111: 3338–3343. doi:10.1073/pnas.1315667111. PMID:24516144.
- Hawbaker, T.J., Keuler, N.S., Lesak, A.A., Gobakken, T., Contrucci, K., and Radeloff, V.C. 2009. Improved estimates of forest vegetation structure and biomass with a LiDAR-optimized sampling design. J. Geophys. Res.: Biogeosci. 114(G2): G00E04. doi:10.1029/2008JG000870.
- Hayashi, R., Kershaw, J.A., and Weiskittel, A. 2015. Evaluation of alternative methods for using LiDAR to predict aboveground biomass in mixed species and structurally complex forests in northeastern North America. Math. Comput. For. Nat.-Resour. Sci. 7: 49–65.
- Hayashi, R., Weiskittel, A., and Kershaw, J.A., Jr. 2016. Influence of prediction cell size on LiDAR-derived area-based estimates of total volume in mixed-species and multicohort forests in northeastern North America. Can. J. Remote Sens. 42: 473–488. doi:10.1080/07038992.2016.1229597.
- Hill, R.A., and Broughton, R.K. 2009. Mapping the understorey of deciduous woodland from leaf-on and leaf-off airborne LiDAR data: a case study in lowland Britain. ISPRS J. Photogramm. Remote Sens. 64: 223–233. doi:10.1016/j.isprsjprs.2008.12.004.
- Hudak, A.T., Crookston, N.L., Evans, J.S., Hall, D.E., and Falkowski, M.J. 2008. Nearest neighbor imputation of species-level, plot-scale forest structure attributes from LiDAR data. Remote Sens. Environ. 112: 2232–2245. doi:10.1016/ i.rse.2007.10.009.
- Hudak, A.T., Strand, E.K., Vierling, L.A., Byrne, J.C., Eitel, J.U., Martinuzzi, S., and Falkowski, M.J. 2012. Quantifying aboveground forest carbon pools and fluxes from repeat LiDAR surveys. Remote Sens. Environ. 123: 25–40. doi:10. 1016/j.rse.2012.02.023.
- Hudak, A.T., Dickinson, M.B., Bright, B.C., Kremens, R.L., Loudermilk, E.L., O'Brien, J.J., Hornsby, B.S., and Ottmar, R.D. 2016. Measurements relating fire radiative energy density and surface fuel consumption — RxCADRE 2011 and 2012. Int. J. Wildland Fire, 25: 25–37. doi:10.1071/WF14159.
- Iverson, L.R., Prasad, A.M., Matthews, S.N., and Peters, M. 2008. Estimating potential habitat for 134 eastern US tree species under six climate scenarios. For. Ecol. Manage. **254**: 390–406. doi:10.1016/j.foreco.2007.07.023.
- Kristensen, T., Næsset, E., Ohlson, M., Bolstad, P.V., and Kolka, R. 2015. Mapping above- and below-ground carbon pools in boreal forests: the case for airborne

- lidar. PLoS One, **10**(10): e0138450. doi:10.1371/journal.pone.0138450. PMID: 26426532.
- Lefsky, M.A., Harding, D., Cohen, W.B., Parker, G., and Shugart, H.H. 1999. Surface LiDAR remote sensing of basal area and biomass in deciduous forests of eastern Maryland, USA. Remote Sens. Environ. 67: 83–98. doi:10.1016/S0034-4257(98)00071-6.
- Li, A., Glenn, N.F., Olsoy, P.J., Mitchell, J.J., and Shrestha, R. 2015. Aboveground biomass estimates of sagebrush using terrestrial and airborne LiDAR data in a dryland ecosystem. Agric. For. Meteorol. 213: 138–147. doi:10.1016/j.agrformet. 2015.06.005
- Liaw, A., and Wiener, M. 2002. Classification and regression by randomForest. R News, 2/3: 18–22.
- Lu, X., Guo, Q., Li, W., and Flanagan, J. 2014. A bottom-up approach to segment individual deciduous trees using leaf-off lidar point cloud data. ISPRS J. Photogramm. Remote Sens. 94: 1–12. doi:10.1016/j.isprsjprs.2014.03.014.
- Martinuzzi, S., Vierling, L.A., Gould, W.A., Falkowski, M.J., Evans, J.S., Hudak, A.T., and Vierling, K.T. 2009. Mapping snags and understory shrubs for a LiDAR-based assessment of wildlife habitat suitability. Remote Sens. Environ. 113: 2533–2546. doi:10.1016/j.rse.2009.07.002.
- Mascaro, J., Asner, G.P., Knapp, D.E., Kennedy-Bowdoin, T., Martin, R.E., Anderson, C., Higgins, M., and Chadwick, K.D. 2014. A tale of two "forests": Random Forest machine learning aids tropical forest carbon mapping. PLoS One, 9(1): e85993. doi:10.1371/journal.pone.0085993. PMID:24489686.
- McGaughey, R.J. 2009. FUSION/LDV: software for LiDAR data analysis and visualization. USDA Forest Service, Pacific Northwest Research Station, Seattle, Wash.
- McNab, W.H. 1989. Terrain shape index: quantifying effect of minor landforms on tree height. For. Sci. 35: 91–104.
- Means, J.E., Hansen, H.A., Koerper, G.J., Alaback, P.B., and Klopsch, M.W. 1994. Software for computing plant biomass — BIOPAK users guide. USDA Forest Service, Pacific Northwest Research Station, Portland, Ore., Gen. Tech. Rep. PNW-GTR-340. doi:10.2737/PNW-GTR-340.
- National Center for Airborne Laser Mapping (NCALM). 2010. Shale Hills 2010 NCALM CZO project report. National Center for Airborne Laser Mapping, Houston, Tex.
- Olden, J.D., Lawler, J.J., and Poff, N.L. 2008. Machine learning methods without tears: a primer for ecologists. Q. Rev. Biol. 83: 171–193. doi:10.1086/587826. PMID:18605534.
- Popescu, S.C. 2007. Estimating biomass of individual pine trees using airborne lidar. Biomass Bioenergy, **31**: 646–655. doi:10.1016/j.biombioe.2007.06.022.
- Popescu, S.C., and Wynne, R.H. 2004. Seeing the trees in the forest. Photogramm. Eng. Remote Sens. 70: 589–604. doi:10.14358/PERS.70.5.589.
- R Core Team. 2016. R: a language and environment for statistical computing. R Foundation for Statistical Computing, Vienna, Austria. Available at http://www.R-project.org/.
- Ruiz-Benito, P., Gómez-Aparicio, L., Paquette, A., Messier, C., Kattge, J., and Zavala, M.A. 2014. Diversity increases carbon storage and tree productivity in Spanish forests. Global Ecol. Biogeogr. 23: 311–322. doi:10.1111/geb.12126.
- Silva, C.A., Hudak, A.T., Klauberg, C., Vierling, L.A., Gonzalez-Benecke, C., de Padua Chaves Carvalho, S., Rodriguez, L.C.E., and Cardil, A. 2017. Combined effect of pulse density and grid cell size on predicting and mapping aboveground carbon in fast-growing *Eucalyptus* forest plantation using airborne LiDAR data. Carbon Balance Manage. 12: 13. doi:10.1186/s13021-017-0081-1.
- Singh, K.K., Davis, A.J., and Meentemeyer, R.K. 2015. Detecting understory plant invasion in urban forests using LiDAR. Int. J. Appl. Earth Obs. Geoinf. 38: 267–279. doi:10.1016/j.jag.2015.01.012.
- Smith, L.A., Eissenstat, D.M., and Kaye, M.W. 2017. Variability in aboveground carbon driven by slope aspect and curvature in an eastern deciduous forest, USA. Can. J. For. Res. 47(2): 149–158. doi:10.1139/cjfr-2016-0147.
- Smith, W.B., and Brand, G.J. 1983. Allometric biomass equations for 98 species of herbs, shrubs, and small trees. USDA Forest Service, North Central Forest Experiment Station, St. Paul, Minn., Res. Note NC-299.
- Swetnam, T.L., Lynch, A.M., Falk, D.A., Yool, S.R., and Guertin, D.P. 2015. Discriminating disturbance from natural variation with LiDAR in semi-arid forests in the southwestern USA. Ecosphere, 6: 1–22. doi:10.1890/ES14-00384.1.
- Tateno, R., Hishi, T., and Takeda, H. 2004. Above- and belowground biomass and net primary production in a cool-temperate deciduous forest in relation to topographical changes in soil nitrogen. For. Ecol. Manage. 193: 297–306. doi:10.1016/j.foreco.2003.11.011.
- van Aardt, J.A., Wynne, R.H., and Scrivani, J.A. 2006. LiDAR-based mapping of forest volume and biomass by taxonomic group using structurally homogenous segments. Photogramm. Eng. Remote Sens. 74: 1033–1044.
- Vierling, K.T., Vierling, L.A., Gould, W.A., Martinuzzi, S., and Clawges, R.M. 2008. Lidar: shedding new light on habitat characterization and modeling. Front. Ecol. Environ. 6: 90–98. doi:10.1890/070001.
- White, J.C., Wulder, M.A., Varhola, A., Vastaranta, M., Coops, N.C., Cook, B.D., Pitt, D., and Woods, M. 2013. A best practices guide for generating forest inventory attributes from airborne laser scanning data using an area-based approach. The Forestry Chronicle, 89(6): 722–723.
- Wing, B.M., Ritchie, M.W., Boston, K., Cohen, W.B., Gitelman, A., and Olsen, M.J. 2012. Prediction of understory vegetation cover with airborne lidar in an

interior ponderosa pine forest. Remote Sens. Environ. 124: 730–741. doi:10. 1016/j.rse.2012.06.024.

- Wolf, J., Brocard, G., Willenbring, J., Porder, S., and Uriarte, M. 2016. Abrupt change in forest height along a tropical elevation gradient detected using airborne lidar. Remote Sens. 8: 864. doi:10.3390/rs8100864.
- Woodbury, P.B., Smith, J.E., and Heath, L.S. 2007. Carbon sequestration in the US forest sector from 1990 to 2010. For. Ecol. Manage. 241: 14–27. doi:10.1016/j.foreco.2006.12.008.
- Wulder, M.A., White, J.C., Nelson, R.F., Næsset, E., Ørka, H.O., Coops, N.C., Hilker, T., Bater, C.W., and Gobakken, T. 2012. Lidar sampling for large-area forest characterization: a review. Remote Sens. Environ. 121: 196–209. doi:10. 1016/j.rse.2012.02.001.
- Xu, Y., Franklin, S.B., Wang, Q., Shi, Z., Luo, Y., Lu, Z., Zhang, J., Qiao, X., and
- Jiang, M. 2015. Topographic and biotic factors determine forest biomass spatial distribution in a subtropical mountain moist forest. For. Ecol. Manage. **357**: 95–103. doi:10.1016/j.foreco.2015.08.010.
- Zald, H.S., Spies, T.A., Seidl, R., Pabst, R.J., Olsen, K.A., and Steel, E.A. 2016. Complex mountain terrain and disturbance history drive variation in forest aboveground live carbon density in the western Oregon Cascades, USA. For. Ecol. Manage. 366: 193–207. doi:10.1016/j.foreco.2016.01.036. PMID:27041818.
- Zhao, K., Popescu, S., and Nelson, R. 2009. LiDAR remote sensing of forest biomass: a scale-invariant estimation approach using airborne lasers. Remote Sens. Environ. 113: 182–196. doi:10.1016/j.rse.2008.09.009.
- Zolkos, S.G., Goetz, S.J., and Dubayah, R. 2013. A meta-analysis of terrestrial aboveground biomass estimation using lidar remote sensing. Remote Sens. Environ. 128: 289–298. doi:10.1016/j.rse.2012.10.017.